Shankar Verma, Amrit; Jiang, Zhiyu; Ren, Zhengru; Hu, Weifei; Teuwen, Julie J.E.

**Important note**
To cite this publication, please use the final published version (if applicable).
Please check the document version above.

# Effects of Onshore and Offshore Environmental Parameters on the Leading Edge Erosion of Wind Turbine Blades: A Comparative Study

**Amrit Shankar Verma**[1]
Faculty of Aerospace Engineering,
Delft University of Technology (TU Delft),
Delft, The Netherlands
e-mail: a.s.verma@tudelft.nl

**Zhiyu Jiang**
Department of Engineering Sciences,
University of Agder,
Grimstad, Norway
e-mail: zhiyu.jiang@uia.no

**Zhengru Ren**
Department of Marine Technology,
Norwegian University of Science and Technology (NTNU),
Trondheim, Norway
e-mail: zhengru.ren@ntnu.no

**Weifei Hu**
State Key Laboratory of Fluid Power and Mechatronic Systems,
School of Mechanical Engineering,
Zhejiang University,
Hangzhou, China
e-mail: weifeihu@zju.edu.cn

**Julie J. E. Teuwen**
Faculty of Aerospace Engineering,
Delft University of Technology (TU Delft),
Delft, The Netherlands
e-mail: j.j.e.teuwen@tudelft.nl

*The presence of rain-induced leading edge erosion of wind turbine blades (WTBs) necessitates the development of erosion models. One of the essential parameters for erosion modeling is the relative impact velocity between rain droplets and the rotating blade. Based on this parameter, the erosion damage rate of a WTB is calculated to estimate the expected leading edge lifetime. The environmental conditions that govern this parameter have site-specific variations, and thus, rain and wind loading on a turbine differ for onshore and offshore locations. In addition, there are wave loads present in the offshore environment. The present paper tries to provide guidelines for erosion modeling and investigates whether there are differences in erosion of blades due to (1) varying rainfall conditions modeled using different droplet size distributions for onshore and offshore locations in combination with (2) winds of varying turbulence intensities and (3) wave-induced loads. Aero-hydro-servo-elastic simulations are carried out for an onshore wind turbine (WT) and a mono-pile-supported offshore WT. Furthermore, erosion variables such as the relative impact velocities and the associated erosion damage rate of a blade are analyzed for various blade azimuth angles. The study shows that the rainfall intensity and turbulence intensity minorly influence the impact velocity and pressure but have a substantial effect on the overall erosion damage rate. Additionally, a significantly higher erosion damage rate is found for blades exposed to offshore rainfall conditions than for blades under onshore rainfall conditions. Furthermore, no substantial influence on erosion is found because of wave-induced loads.* [DOI: 10.1115/1.4049248]

## Introduction

The consistent demand for the reduction of carbon footprint in the energy sector has motivated power production from sustainable sources such as wind, hydro, wave, and solar power sources [1]. Among the different resources, wind energy is one of the most reliable and readily available power sources and can be harnessed using wind turbines (WTs) [2,3] (Fig. 1(*a*)).[2] Given that the power extracted from the WT increases with the rotor swept area along with the cube of the wind speed, large WTs are currently in high demand both in onshore and offshore sectors [4,5]. Another major advantage that drives the design of large-sized WTs is the reduced operation and maintenance costs [6]. This upscaling in the size of WTs is profitable. However, it poses several engineering challenges. For instance, latest generation of wind turbine blades (WTBs) rotates with tip speeds in the range of 0–120 m/s and is exposed to high velocity impact with rain droplets during precipitation. The recurring high velocity impacts between rain droplets and rotating blades during their service life exert cyclic fatigue stresses on the WTBs. This eventually leads to the leading edge erosion (LEE) of WTBs

that includes development of pitting and surface cracks at the leading edge (Fig. 1(*b*)).[3] In severe cases, the damage could even penetrate into the composite substrate (Fig. 1(*b*)) [7,8].

Leading edge erosion of a WTB is a critical issue to the WT performance. LEE causes the local roughening of surfaces, which in turn provokes the premature transition of laminar flow into turbulent flow along the leading edge, thereby reducing the aerodynamic efficiency and annual energy production (AEP) of a turbine [9]. In general, regular inspection, maintenance, and repair of WTBs due to LEE are inevitable to keep up with the target AEP of a turbine through the design life, thereby increasing the cost of wind energy. It has been reported by Herring et al. [9] and Wiser et al. [10] that repair and maintenance due to LEE cost the European offshore WT sector more than £56 million annually. Therefore, LEE of WTBs requires immediate attention.

Several research efforts are being made to address the issue of LEE due to high velocity rain droplet impact. These include developing, testing, and comparing leading edge coating systems in accelerated rain erosion tests and quantifying their rain erosion resistance in excess of 100–200 m/s droplet impact [11–13]. Another aspect for controlling rain erosion of a WTB is to develop a control algorithm [14], which automatically reduces the tip speed of the blade (and thus the impact velocity) in the event

---

[3]https://www.tno.nl and http://www.duraledge.dk
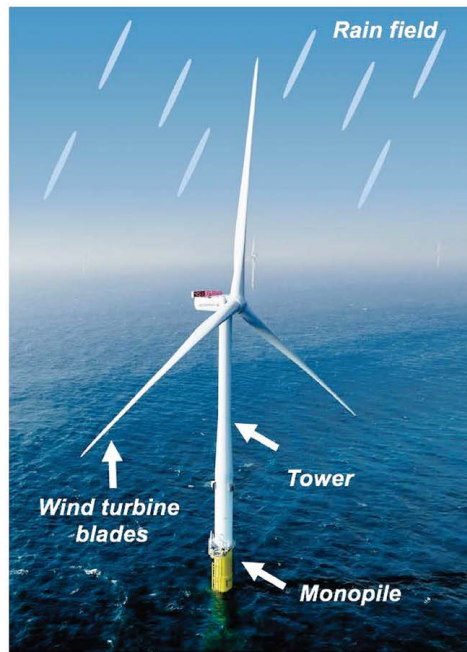
**Fig. 1** (a) WT exposed to rain field (picture modified from Vattenfall group) and (b) LEE of WTBs (adapted from the TNO and DUR-ALEDGE project)
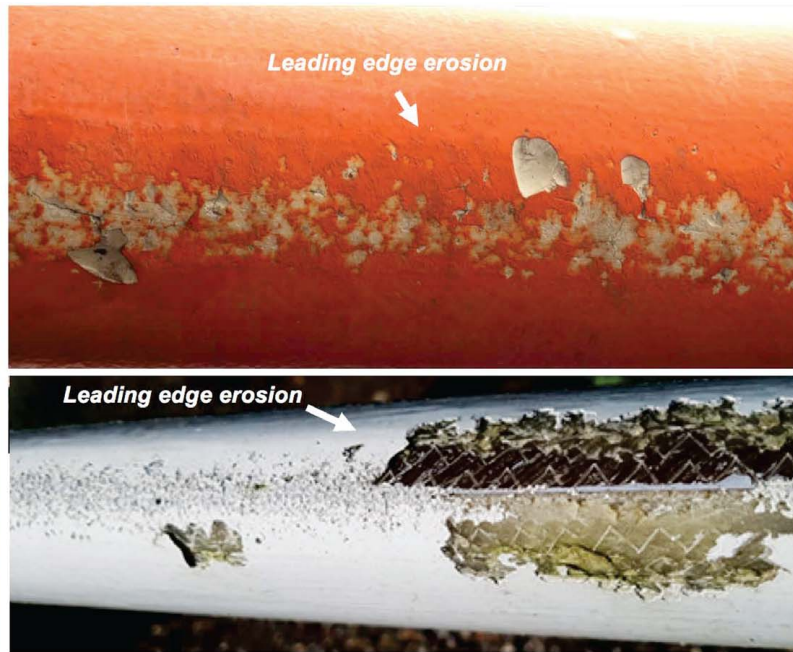
of harsh precipitation, thereby inhibiting cumulative fatigue damage accumulation due to repeated rain droplet impact. Computational models [7,15] are also being developed where emphasis is on estimating the fatigue life based on cyclic stresses induced on the leading edge over its service life.

Amirzadeh et al. [16] developed a computational framework to estimate the fatigue life of a blade, where erosion damage rates for the leading edge under varying impact velocities and different rainfall conditions were evaluated. Similar studies can also be found in Refs. [12,17–19], where fluid structure interaction

models are developed using sophisticated numerical codes. However, one of the simplifications in all the previous studies is that a maximum impact velocity between 100 and 140 m/s is simply assumed for analysis purposes, and the effects of droplet impact angles, blade surface curvature, varying wind speeds, and blade rotation are ignored. In principle, for the fatigue design of the coating material, it is essential to quantify the impact velocity and cyclic variation during blade rotation as well as their dependence on the rainfall intensity, droplet impact angle, and wind condition to which a WTB is exposed. It has been shown in the
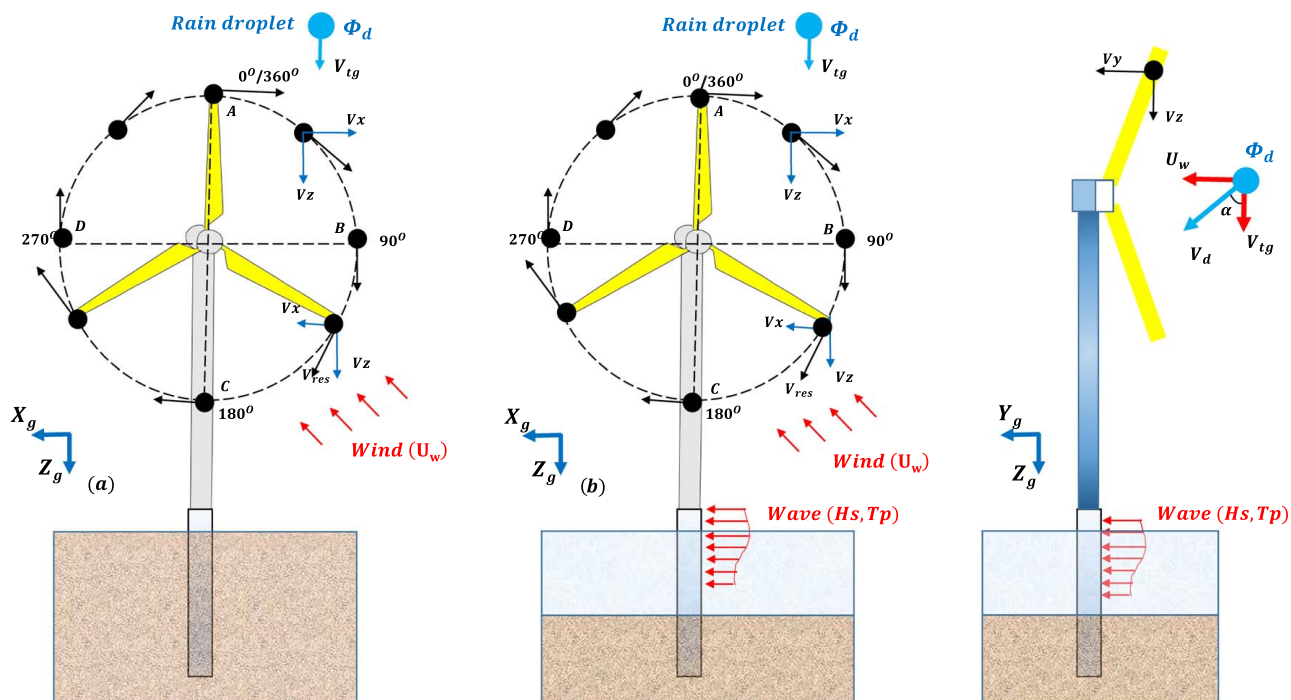


**Fig. 2** Different input variables related to onshore and offshore WTs and definition of impact angle $\alpha$

literature [8,13,20] that the erosion damage rate ($\dot{D}_i$) of the leading edge modeled as a flat surface is proportional to the 6.7th power of the impact velocity ($|\vec{V}_{imp}|^{6.7}$). Therefore, this makes the relative impact velocity between rain droplets and the rotating blade an essential parameter for erosion modeling and damage prediction of the leading edge of the WTB.

The environmental conditions that govern the above-mentioned erosion parameters have site-specific variations, and thus, rain and wind loading on a turbine differ for onshore and offshore locations. For instance, less turbulent winds are present in the offshore environment together with rainfall having varying statistical characteristics at onshore and offshore locations [21]. In addition, there are wave loads present in the offshore environment (Fig. 2) that can cause additional dynamic responses in the WT and can affect the overall erosion damage rate of WTBs. Thus, the present paper tries to provide guidelines for erosion modeling and investigates whether there are differences in erosion of blades due to (1) varying rainfall conditions modeled using different droplet size distributions (DSDs) for onshore and offshore locations in combination with (2) winds of varying turbulence intensities and (3) wave-induced loads. The aim of the paper is to provide guidelines on whether all these parameters need to be included for site-specific LEE modeling. For this purpose, aero-hydro-servo-elastic simulations are carried out for an onshore WT and a monopile-supported offshore WT, both having similar turbine settings of an National Renewable Energy Laboratory (NREL) 5 MW open-source WT. Realistic environmental conditions are modeled separately for both onshore and offshore locations, and erosion variables such as the impact velocities and the associated erosion damage rate of a blade are analyzed. In addition, an assessment is presented at varying blade azimuth angles. The next section describes in detail the problem definition and the analysis procedure.

## Problem Definition and Analysis Procedure

There are two main erosion parameters that are of interest in this paper for studying the effects of environmental parameters on the erosion of onshore and offshore WTBs. These parameters include (a) the relative impact velocity between rain droplets and rotating blades ($\vec{V}_{imp}$) and (b) the associated erosion damage rate of the rotating blade contributed from the repetitive impact with the rain droplets ($\dot{D}_i$). Principally, these parameters depend primarily on the statistics of the environmental conditions to which a WT is exposed during its service life (see Fig. 3). The parameters are described through (1) rain statistics that are defined by two statistical parameters—the rainfall intensity ($I$), which is defined as the total accumulated rainfall in a given period of time expressed in mm/h, and rain droplet size ($\phi_d$), which represents the diameter of rain droplets in a given rain. Furthermore, (2) wind statistics are described by the mean wind speed ($U_w$) and turbulence intensity ($TI$), and (3) wave statistics are described based on the significant wave height ($H_s$) and wave spectral peak period ($T_p$). Figure 3 also shows other parameters that are derived from the rain and wind statistics and are essential for erosion modeling, such as the number of drops for a given instance of rain ($q$), the droplet speed ($V_d$), and the droplet impact angle ($\alpha$). The discussions about how these parameters are calculated in this paper are mentioned in the subsequent sections. In addition, it is also essential to define the steady-state rotor speed–wind speed curve of the WT that decides the tip speed of the blade for a given wind speed. Note that for a given WT and as a result of these statistical parameters, $\vec{V}_{imp}$ is expected to vary with the blade azimuth angle ($\theta \in [0 \text{ deg}, 360 \text{ deg}]$) and different radial positions ($r$) along the blade length ($l$).

**Relative Impact Velocity Between Rain Droplets and the Rotating Blade ($\vec{V}_{imp}$).** The relative impact speed between a falling rain droplet and a rotating blade can be expressed as follows (see the velocity triangle in Fig. 2):

$$|\vec{V}_{imp}| = \sqrt{(V_x)^2 + (V_y - V_d \sin \alpha)^2 + (V_z - V_d \cos \alpha)^2} \quad (1)$$
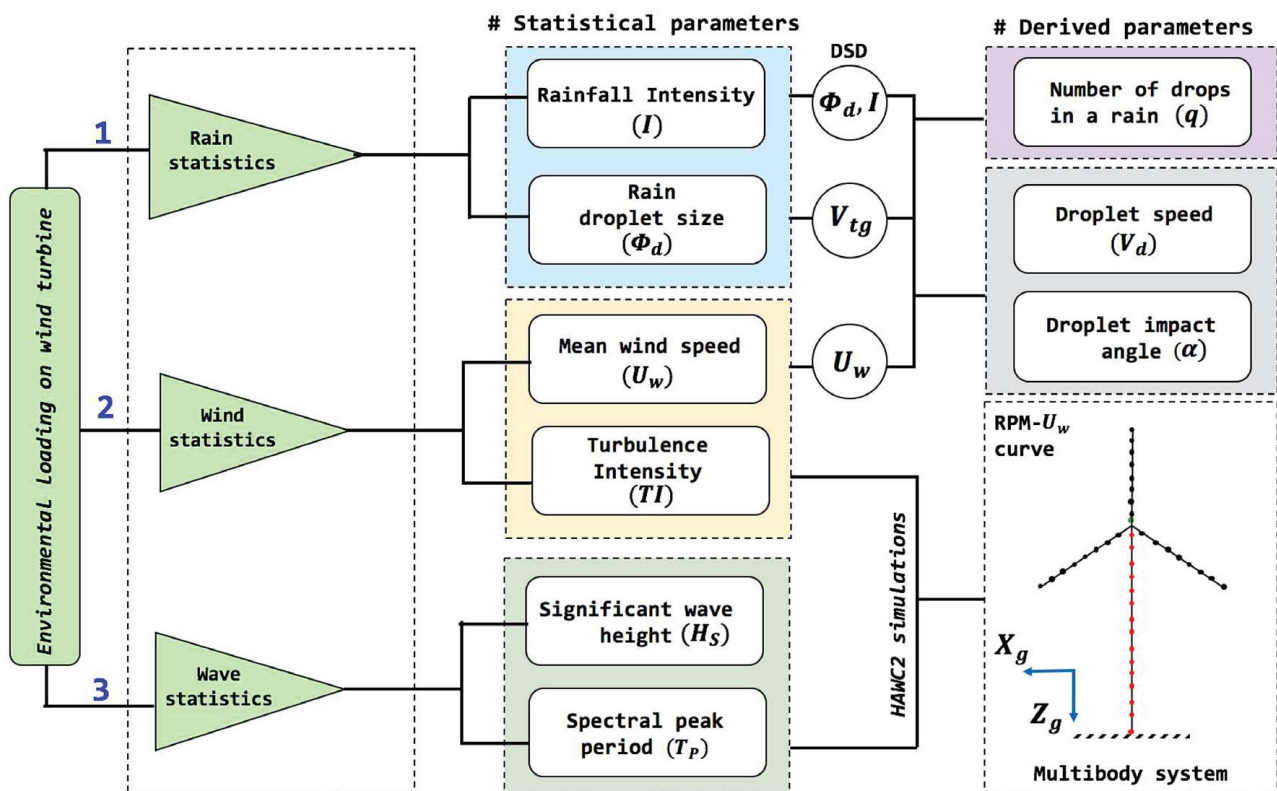


**Fig. 3   Flowchart showing different source of environmental loads on WT and associated statistical parameters**
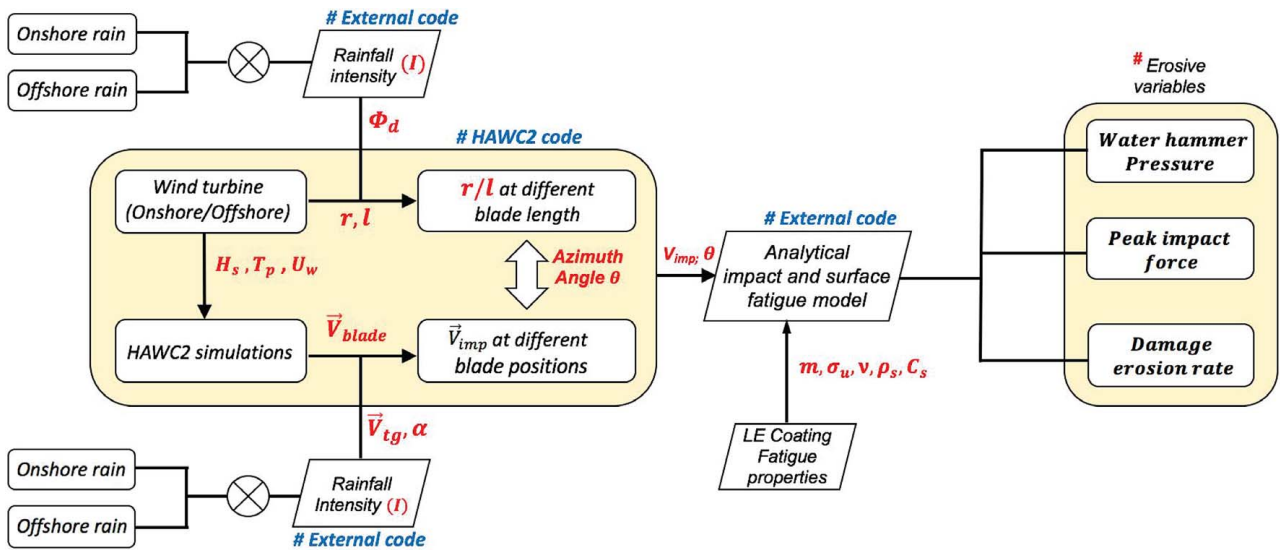
**Fig. 4  Analysis procedure considered in the study**

where $V_x$, $V_y$, and $V_z$ are the absolute velocity components of the blade in the global frame $X_g$, $Y_g$, and $Z_g$ directions and $V_d$ is the assumed droplet speed in the same frame. $V_d$ is defined as (Fig. 2) [22]

$$V_d = \sqrt{U_w^2 + V_{tg}^2} \qquad (2)$$

$\alpha$ is defined as the droplet impact angle and is defined as [22] (see Fig. 2)

$$\alpha = \arctan\left(\frac{U_w}{V_{tg}}\right) \qquad (3)$$

where $V_{tg}$ is defined as the vertical terminal speed of a rain droplet, and its magnitude is given by

$$V_{tg} = 9.65 - 10.3e^{-0.6\phi_d} \quad (0.5\,\text{mm} < \phi_d < 5\,\text{mm}) \qquad (4)$$

Note that in the above equations, $U_w$ is the horizontal mean wind speed and is considered the component of the rain droplet velocity in the $Y_g$ direction. On the other hand, $V_{tg}$ is defined as the vertical terminal speed of a rain droplet and is considered the component of the rain droplet velocity in the $Z_g$ direction. This is considered for simplicity; nevertheless, the actual droplet impact angle and droplet velocity components may deviate because of the influence of the rotating blades on the induced velocities.

A list of assumptions that are considered in Eqs. (1)–(4) are summarized as follows:

(1) The axial and circumferential inductions of the air flow are ignored for the estimation of the droplet velocity, and it is approximated as the sum of the freestream wind velocity ($U_w$) and the terminal velocity ($V_{tg}$).
(2) WTB is modeled as a rotating line body (1D geometry) and the surface is modeled as flat while computing erosion damage rate. Also, the impact angle described through Eq. (3) neglects the effects of the blade surface curvature.
(3) The local transport and trajectory deviation of raindrops due to the aerodynamic field around the blade section are neglected.

*Droplet Size Distribution: Onshore and Offshore Rainfall.* There exists a probabilistic distribution of droplet diameter ($\phi_d$) in a given rain, which is related to the rainfall intensity ($I$) through a DSD. In general, this distribution varies for onshore and offshore rainfall conditions. The rainfall scenario for the onshore condition is defined using Best's distribution, which is given by [23]

$$F(\phi_d) = 1 - \exp\left[-\left(\frac{\phi_d}{1.3I^{0.232}}\right)^{2.25}\right] \qquad (5)$$

Similarly, for representing the rainfall scenario for the offshore conditions, the DSD is given by [21]

$$F(\phi_d) = 1 - \exp\left[-\left(\frac{\phi_d}{1.03I^{0.138}}\right)^{2.83I^{-0.0953}}\right] \qquad (6)$$

where $F(\phi_d)$ is the cumulative distribution function (CDF) of the droplet size. In Eqs. (5) and (6), the droplet diameter $\phi_d$ is expressed in mm, whereas $I$ is expressed in mm/h. Note that the offshore DSD, shown in Eq. (6), was recently developed by Herring et al. [21], where a CDF for $\phi_d$ based on one year of measured data was derived for offshore conditions and compared with the estimates from Best's DSD [23]. Notable differences were found between the distributions with droplet sizes overestimated using Best's DSD [23]. However, it should be noted that the data for analysis in Ref. [21] for offshore conditions are based on only one year of recorded data and require further improvement. Therefore, in this study, Best's distribution [23] is used to represent rainfall scenarios at both onshore and offshore locations for all cases, and a representative droplet size is selected for different $I$. However, a standalone comparative study is performed in this paper to exclusively check the effect of varying DSDs for onshore and offshore conditions on the LEE of WTBs. Note that the use of these DSDs includes a few assumptions; for instance, droplets are assumed to be spherical for all cases, and the effects of changes in the shape of the droplets, especially for higher rainfall intensities, are neglected.

All the variables discussed through these equations are also marked in a flowchart shown in Fig. 4, where the analysis framework of the study is described. First, aero-hydro-servo-elastic simulations are carried out in HAWC2 [24] for a rotating blade based on the NREL 5 MW turbine [25] by considering realistic

**Table 1  Material properties for the coating material [11]**

| Parameter | Values | Units |
| --- | --- | --- |
| $\rho_s$ | 1320 | kg/m³ |
| $c_s$ | 2480 | m/s |
| $\sigma_u$ | 57.6 | MPa |
| $m$ | 14.9 | – |
| $\nu$ | 0.395 | – |

**Table 2    Description of the NREL 5-MW reference turbine [25]**

| Rating | 5 MW turbine |
| --- | --- |
| Rotor orientation and configuration | Upwind, three blades |
| Control variable speed | Collective pitch |
| Drive train high speed | Multiple-stage gearbox |
| Rotor and hub diameter | 126 m and 3 m |
| Hub height | 90 m |
| Cut-in, rated, and cut-out wind speed | 3 m/s, 11.4 m/s, and 25 m/s |
| Cut-in and rated rotor speed | 6.9 rpm and 12.1 rpm |
| Rated tip speed | 80 m/s |
| Rotor mass | 110,000 kg |
| Nacelle mass | 240,000 kg |
| Tower mass | 347,460 kg |

environmental conditions for land-based WT and monopile-supported offshore WT. From the analysis, the rotational speed of the blade is evaluated at different $\theta$ along the blade span length ($r/l$). Furthermore, these results are combined with an in-house external code describing rainfall parameters $\phi_d$, $I$, $\alpha$, and $V_{tg}$, and $|\vec{V}_{imp}|$ is estimated using Eq. (1). The details of the environmental load cases considered in this study are described in the next section. Once $|\vec{V}_{imp}|$ is evaluated, the structural responses of the leading edge due to rain droplet impact are evaluated using different erosion variables and are discussed below.

**Peak Impact Forces, Impact Pressure, and Associated Leading Edge Erosion Damage Rate ($\dot{D}_i$).** The following are the LE structural response parameters that are used to quantify LEE damage: (a) peak impact forces ($F_{imp}$), (b) water hammer pressure ($p_{wh}$), and (c) erosion damage rate ($\dot{D}_i$) (Fig. 4). The $F_{imp}$ on the blade's leading edge is given by an analytical model developed in Refs. [26,27]. The analytical model is verified in our previous work for WTBs [17], and $F_{imp}$ is given as

$$F_{imp} = 0.84 \, \rho_w \, |\vec{V}_{imp}|^2 \, \phi_d^2 \tag{7}$$

where $\rho_w$ is the density of water taken as 1000 kg/m³. Furthermore, the erosion damage rate is defined by an analytical surface fatigue damage model developed and validated in Refs. [8,13]. The model applies Miner's rule to estimate $\dot{D}_i$ and is given by

$$\dot{D}_i = \frac{\dot{N}}{N_{ic}} = \frac{q|\vec{V}_{imp}|\beta_d}{(8.9/\phi_d^2)(S/p_{wh})^{5.7}} \tag{8}$$

where $\dot{D}_i \geq 1$ represents fatigue damage and $q$ is the number of droplets per unit volume of rainfall, which is given by

$$q = 530.5 \frac{I}{V_{tg}\phi_d^3} \tag{9}$$

where $I$ is defined in mm/h, $\phi_d$ is defined in mm, and $V_{tg}$ is defined in m/s. It should be noted that the above equation for $q$ corresponds to the ideal rainfall conditions where it is assumed that all the droplets in an event of rain have a size equal to the median droplet diameter that is estimated from a given DSD and rain intensity ($I$). $\beta_d$ is the impingement efficiency given by the relation

$$\beta_d = 1 - e^{-15\phi_d} \tag{10}$$

$p_{wh}$ is the water hammer pressure defined as

$$p_{wh} = \frac{\rho_w c_w |\vec{V}_{imp}|}{1 + (\rho_w c_w / \rho_s c_s)} \tag{11}$$

where $\rho_s$ and $c_s$ are the density and speed of sound in the coating material, respectively. $S$ is the erosive strength of the coating material defined as

$$S = \frac{4\sigma_u(m-1)}{1 - 2\nu} \tag{12}$$

where $\sigma_u$, $m$, and $\nu$ are the ultimate strength, Wöhler slope, and Poisson's ratio of the coating material, respectively. In this study, a polyethylene terephthalate (PET)-based thermoplastic coating material [11] is used to determine the erosion damage rate. The material properties are tabulated in Table 1.

## Material and Modeling Method

A generic 5 MW-based WT originally designed by NREL is modeled in aeroelastic HAWC2 code [24] for estimating the global motion responses of the rotating blade for both onshore and offshore WTs. The code is based on multibody dynamics
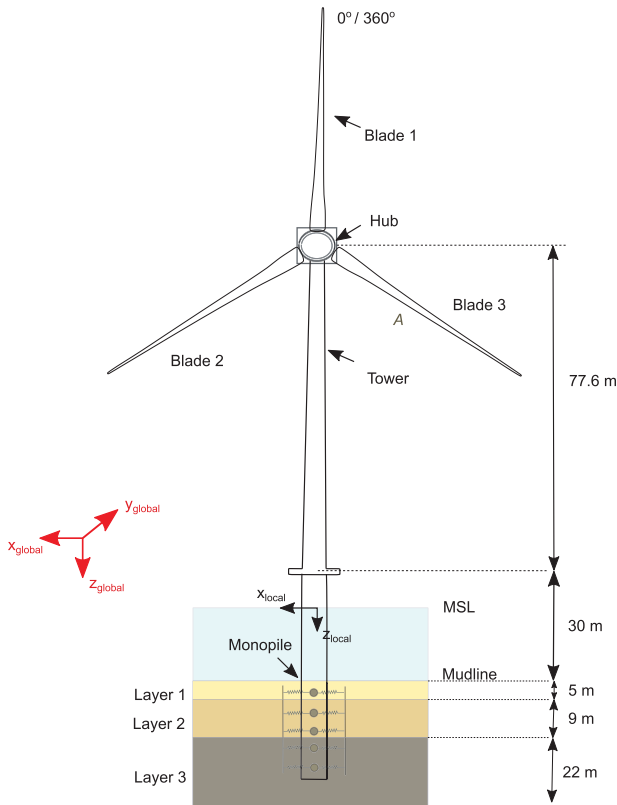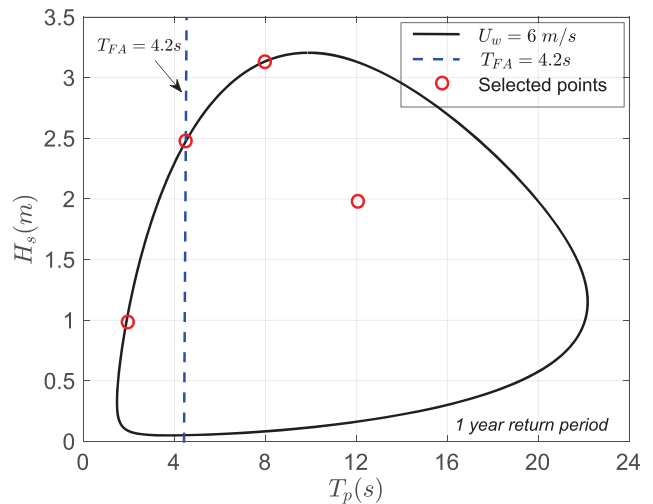


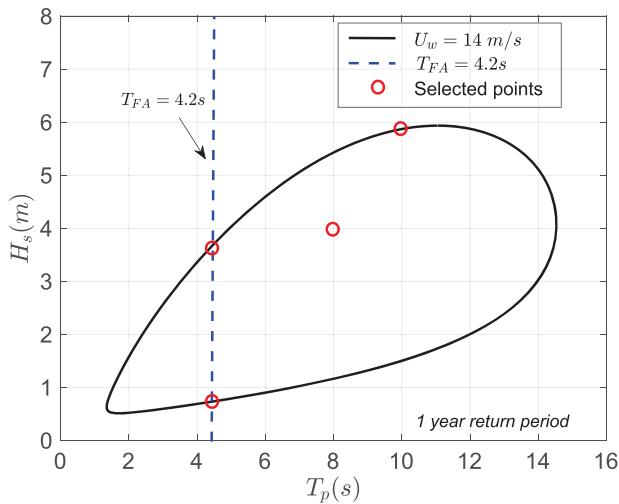**Fig. 5 Numerical model considered in HAWC2 for the offshore WT**
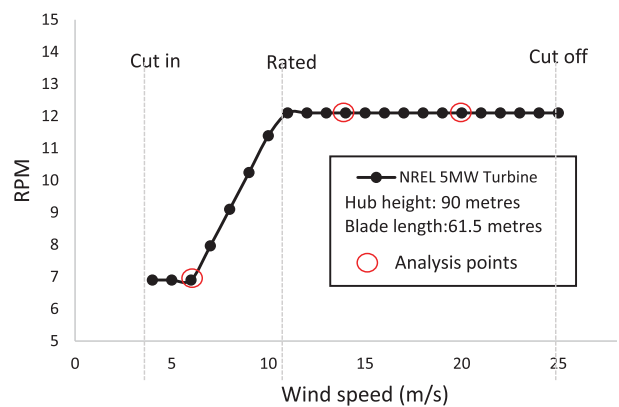


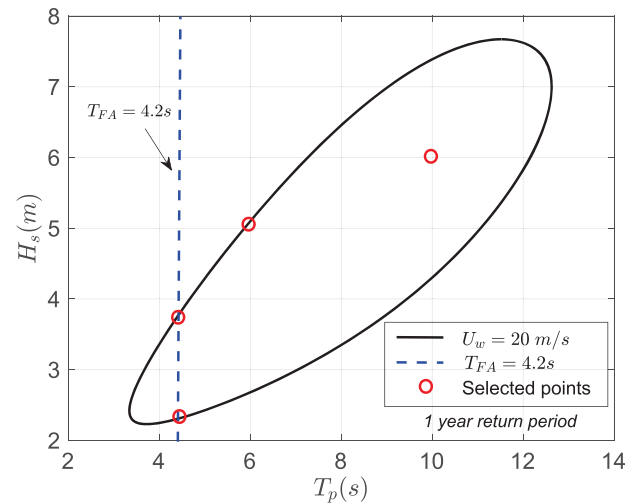**Fig. 6 Rotor speed–mean wind speed curve for the NREL 5MW WT**
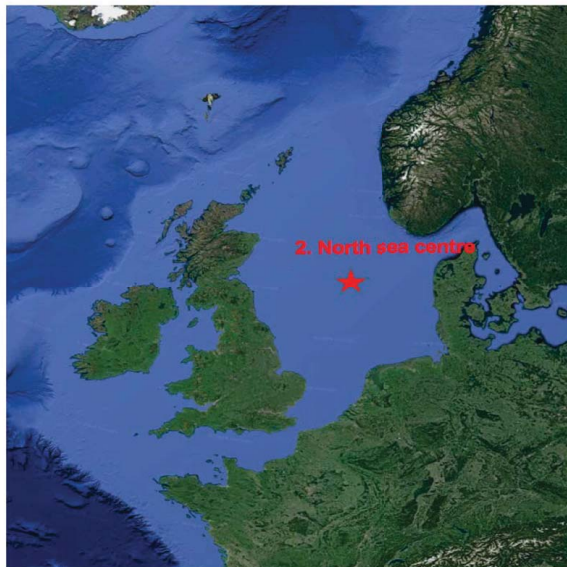
**Fig. 7 (a) North sea center offshore site; 2D contour surface for $H_s$, $T_p$ for (b) $U_w = 6$ m/s, (c) $U_w = 14$ m/s, and (d) $U_w = 20$ m/s and selected load cases**

where structural systems can be discretised with Timoshenko beam elements and components of the turbine can be connected together through constraints or joints. The code is able to simulate time domain responses of WTs under the action of aerodynamic and hydrodynamic loads. The design parameters for the NREL 5 MW WT are provided in Table 2.

Figure 5 presents the numerical model for the offshore WT considered in the study, where the NREL 5 MW turbine [25] is adapted based on the phase II model of offshore code comparison (OC3) [28]. Realistic soil properties are defined for the monopile, having a diameter of 9 m.

An eigenfrequency analysis is performed for the offshore WT, and the natural period in the first fore-aft and side-side bending modes is found to be approximately 4.2 s ($T_{FA}$, $T_{SS} = 4.2$ s). It should be noted that in the original OC3 model, the damping ratio of the first fore-aft and side-side bending mode of the turbine is close to 0.2%, which is tuned to a value of 1% critical in this study as per recommendations and experimental observations from Ref. [29]. The structural components, including blades, monopiles, and towers, are modeled using Timoshenko beam

elements, and the soil is defined through distributed springs. The hydrodynamic loads on the monopile are calculated by Morison's equation [30], and the JONSWAP spectrum [31] is used to generate the irregular waves. Furthermore, in HAWC2 simulations [32], aerodynamic loads on the blade are evaluated using blade element momentum (BEM) theory with engineering corrections. The BEM implemented in HAWC2 includes several engineering models, such as dynamic inflow (dynamic induction), skew inflow, dynamic stall, and the near-wake models. The efficiency of these models in HAWC2 is validated against the computational fluid dynamics and the advanced vortex model for blade loads and axial induction; see Refs. [33,34]. However, BEM cannot account for advanced flow effects such as wake rotation and hence may affect the local flow phenomenon, but the corrected BEM is still useful for engineering aeroelastic analysis. Furthermore, inflow wind turbulence is generated using Mann's turbulence box [35] in the HAWC2 code, and the effects of wind shear are included. The details of the parameters used for generating the turbulence can be found in another work [2,36]. Additionally, the model for the onshore WT is similar to the offshore WT except that

**Table 3  Load cases considered for the analysis**

| EC | $U_w$ (m/s) | TI | $H_s$ (m) | $T_p$ (s) |
|---|---|---|---|---|
| EC1 | 6 | 0, 0.06, 0.12, 0.26 | 1.00 | 2.00 |
| EC2 | 6 | 0, 0.06, 0.12, 0.26 | 2.30 | 4.20 |
| EC3 | 6 | 0, 0.06, 0.12, 0.26 | 3.14 | 8.00 |
| EC4 | 6 | 0, 0.06, 0.12, 0.26 | 2.00 | 12.00 |
| EC5 | 14 | 0, 0.06, 0.12, 0.26 | 0.70 | 4.20 |
| EC6 | 14 | 0, 0.06, 0.12, 0.26 | 3.50 | 4.20 |
| EC7 | 14 | 0, 0.06, 0.12, 0.26 | 4.00 | 8.00 |
| EC8 | 14 | 0, 0.06, 0.12, 0.26 | 6.00 | 10.00 |
| EC9 | 20 | 0, 0.06, 0.12, 0.26 | 2.27 | 4.20 |
| EC10 | 20 | 0, 0.06, 0.12, 0.26 | 4.90 | 4.20 |
| EC11 | 20 | 0, 0.06, 0.12, 0.26 | 5.00 | 6.00 |
| EC12 | 20 | 0, 0.06, 0.12, 0.26 | 6.00 | 10.00 |

(1) the tower of the land-based turbine is rigidly connected at the bottom and (2) there are no hydrodynamic loads acting on the turbine.

### Environmental Load Cases

*Wave and Wind Conditions.* To analyze LEE subjected to rain droplet impact for both onshore and offshore WTs, three different mean wind speeds, i.e., $U_w = 6$, 14, 20 m/s, are considered in this study. These cases range between the cut-in and rated wind (Fig. 6) speed of a turbine ($U_w = 6$ m/s), the rated and cutoff speed ($U_w = 14$ m/s), and a speed that is closer to the cutoff speed ($U_w = 20$ m/s). Furthermore, for each case of $U_w$, four different turbulence intensities (TI) are considered (TI = 0, 0.06, 0.12, 0.26). These values represent steady wind and wind with low, medium, and high turbulence, respectively. For instance, TI = 0.06 represents the turbulence level at which the offshore WT operates, while TI = 0.26 corresponds to inflow wind conditions during gusts and storms.

To consider the effect of wave-induced loads on the offshore WT, the North Sea centre is considered as a representative offshore site (Fig. 7(a)), and the 2D contour surface [3] for different combinations of significant wave heights ($H_s$) and wave spectral peak periods ($T_p$) for a chosen $U_w$ are shown in Figs. 7(b)–7(d). The dots in Figs. 7(b)–7(d) correspond to the selected load cases for the offshore WT. Note that the points where the vertical line intersects the contour surface correspond to the case close to the highest resonance frequency of the turbine ($T_{FA} = 4.2$ s). Overall, 12 load environmental cases (EC1 to EC12) are considered and are given in Table 3. Additionally, for each load case, 20 random seeds were analyzed to consider the statistical uncertainty. The random seeds were considered in this study for the generation of turbulence boxes as well as for generating irregular waves using the JONSWAP spectrum [31] with different seed numbers. Each analysis ran for 4000 s, where the first 400 s were filtered out to avoid start-up effects.
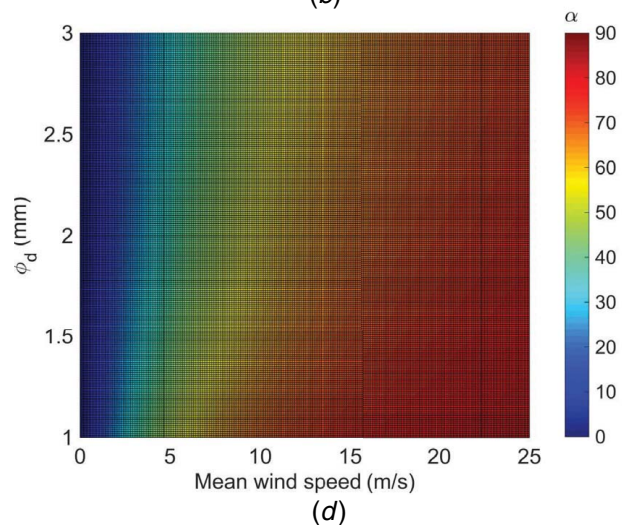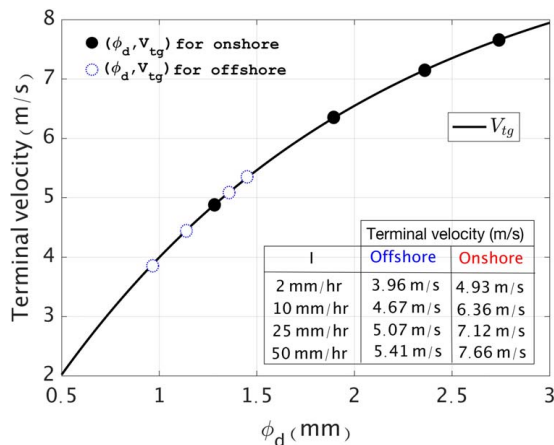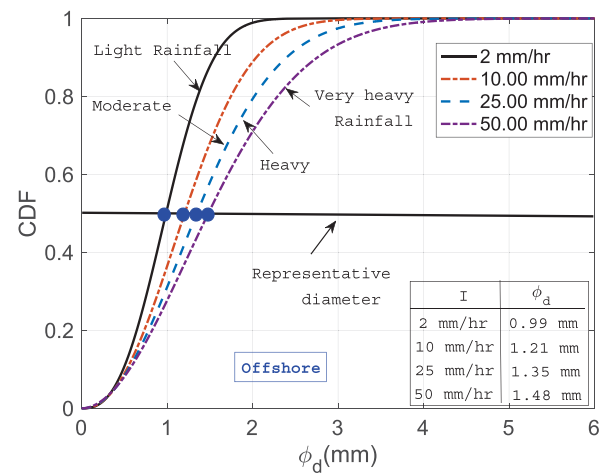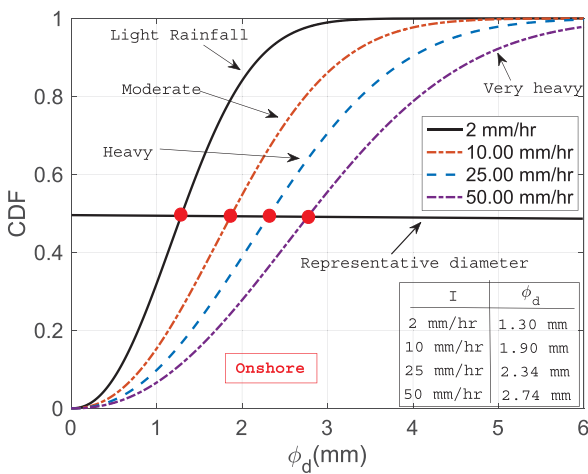


**Fig. 8  Choice of $\phi_d$ for different I: (a) onshore—best distribution, (b) offshore—distribution by Ref. [21], (c) $V_{tg}$, and (d) variation of $\alpha$ (deg) with varying $\phi_d$ and $U_w$**
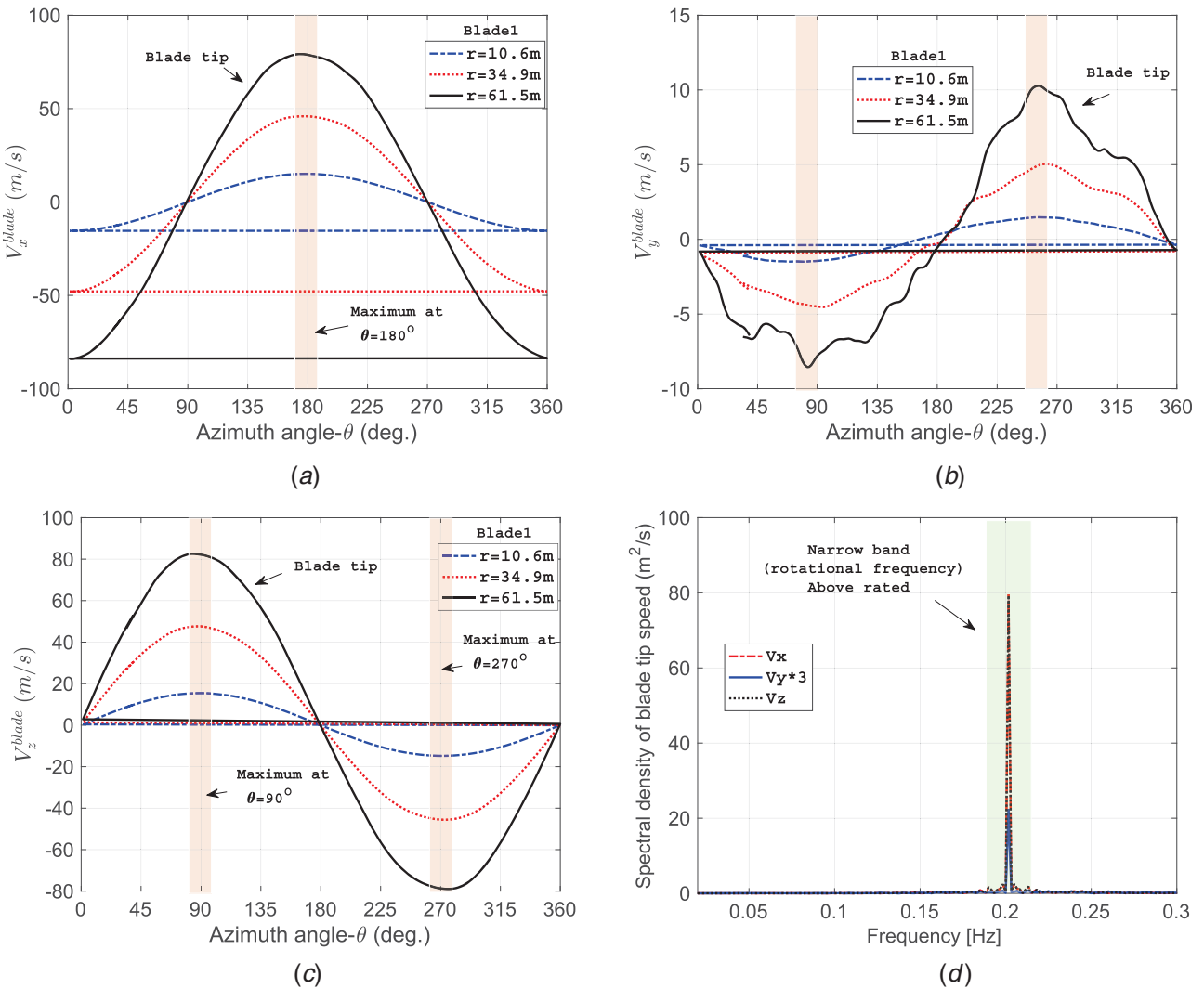
**Fig. 9 Comparison of (a) $V_x^{blade}$, (b) $V_y^{blade}$, (c) $V_z^{blade}$ at different $\theta$ and $r = 10.4$, 34.9, 61.5 m, and (d) spectral density of blade tip speed ($U_w = 20$ m/s)**

*Rainfall Conditions.* As already mentioned before, Best's distribution [23] is used to represent the rainfall scenario under both onshore and offshore conditions, and a suitable droplet size is selected for different values of $I$. Nevertheless, a standalone comparative study is presented separately to determine the effect of DSDs on the LEE of WTBs and how site-specific rainfall conditions can affect the overall LEE. Four different rainfall intensities ($I$) are considered for both onshore and offshore conditions: (1) light rainfall (2 mm/h), (b) moderate rainfall (10 mm/h), (c) heavy rainfall (25 mm/h), and (d) very heavy rainfall (50 mm/h). Based on these values of $I$, the rain droplet size ($\phi_d$) is determined from the DSDs given by Eqs. (5) and (6) for onshore and offshore conditions, respectively, and are shown in Figs. 8(a) and 8(b). The points where the black horizontal line intersects the CDF curve correspond to the representative $\phi_d$ considered in the study, i.e., $\phi_d = 1.30$, 1.90, 2.34, 2.74 mm for different values of $I$ representing onshore conditions and $\phi_d = 0.99$, 1.21, 1.35, 1.48 mm for different values of $I$ representing offshore conditions. It can be seen from these figures that Best's distribution for onshore conditions generally predicts larger droplet size for a given rainfall intensity compared to offshore DSDs, and the differences in their estimates are significant for a higher rainfall intensity. For instance, the percentage difference between the predicted $\phi_d$ for the onshore and offshore rainfall scenarios is approximately 27% and 60% for $I = 2$ mm/h and $I = 50$ mm/h, respectively. Furthermore, $V_{tg}$ are obtained for

different $\phi_d$ based on Eq. (4) for both onshore and offshore conditions and are represented by solid and dashed dots, respectively (Fig. 8(c)). Finally, using Eq. (3), the droplet impact angles ($\alpha$) are obtained for different combinations of $U_w$, $V_{tg}$, and $\phi_d$ and are presented in Fig. 8(d).

## Results and Discussion

In this section, the results for the velocities of the rotating blade are presented first and are discussed at different azimuth angles and radial positions. Furthermore, the effects of the (a) rainfall intensity, (b) wave-induced loads, and (c) turbulence intensity on the impact velocities and erosion damage rates are discussed. Note that for all the cases, "*Blade 1*" of the WT is used for discussion.

**Blade Speed at Different Azimuth Angles ($\theta$) and Radial Positions ($r$).** Figures 9(a)–9(c) present the blade velocity in the global $x$, $y$, and $z$-directions, respectively, for the case of $U_w = 20$ m/s and $TI = 0.06$, corresponding to an onshore WT. The results are presented at different blade azimuth angles ($\theta$) and three different positions along the blade length. The velocity of the rotating blade is highest in the rotor plane ($xz$), with the blade velocity being the largest in the $x$ and $z$ directions. However, the velocity of the blade in the global $y$-direction ($V_y^{blade}$) is

smaller, and its peak value is close to 11 m/s compared to $V_x$ and $V_z$, where the peak velocity can be in the range of 80 m/s. Additionally, as expected, the blade tip shows the largest velocity for all cases and thus will be used for discussion of the results in subsequent sections. Furthermore, the velocity of the blade in the $x$-direction has a positive peak value at $\theta = 180$ deg and a negative peak value at $\theta = 0$ deg. On the other hand, $V_z^{\text{blade}}$ has the highest positive impact velocity at $\theta = 90$ deg and the corresponding negative velocity at $\theta = 270$ deg. This negative velocity at $\theta = 270$ deg is expected to give the largest relative impact velocity between rain and the rotating blade ($\vec{V}_{\text{imp}}$) due to the direction of rainfall in the opposite direction. It is also evident from the figure that $V_z^{\text{blade}}$ shows a perfect smooth sinusoidal curve. However, $V_y^{\text{blade}}$ is affected by $TI$, and thus, a perfect sinusoidal smooth function is not obtained, the effect of which is critical at the blade tip. Nevertheless, the spectral density curve of the blade tip speed shown in Fig. 9($d$) clearly shows narrow band behavior and represents the dominating frequency defined by the power curve of WT.

**Effects of the Rainfall Intensity ($I$).** Figure 10($a$) presents the comparison between the relative impact velocity for the rotating blade tip ($r = 61.5$ m) and a single rain droplet corresponding to different $I = 2$ mm/h, 10 mm/h, 25 mm/h, and 50 mm/h. The results are presented at different values of $\theta \in [0$ deg, 360 deg$]$ and for a case of an onshore WT operating at $U_w = 20$ m/s (i.e., above the rated

wind speed) and having steady wind conditions ($TI = 0$). Note that for all the cases of rainfall intensities and corresponding $U_w$, the droplet impact angle ($\alpha$) varies (see Fig. 8($d$)) and is considered in all the results presented hereafter. It can be seen from the figure that the impact velocity between the blade and the rain droplet varies cyclically, where it is least at approximately $\theta = 90$ deg and highest around $\theta = 270$ deg—a percentage difference of approximately 13% is found between the maximum and minimum values for rainfall conditions representing the largest rainfall intensity ($I = 50$ mm/h). This implies that rain-induced fatigue damage accumulation and the subsequent erosion damage rate of a WTB coating would vary with varying blade azimuth angles traversed during the rotation of the blade.

Furthermore, it is also found that the relative impact velocity between the blade tip and the rain drops increases with increasing rainfall intensity, given that rain corresponding to large rainfall intensity yields a larger droplet size (as seen from DSDs presented before) and therefore is associated with a higher terminal velocity of the drop. Given that $V_y^{\text{blade}}$ and $V_z^{\text{blade}}$ are the dominating blade responses that influence $\vec{V}_{\text{imp}}$ for varying rainfall characteristics (and including $\alpha$ and $V_d$, see Eq. (1)), only these parameters will be considered for the assessment of erosive variables in our subsequent discussions. Therefore, for all the discussions hereafter, the velocity of the blade in the $x$-direction ($V_x^{\text{blade}}$) is filtered out for a lucid scale of comparison among different erosive variables for varying environmental parameters. For instance, Fig. 10($b$) presents
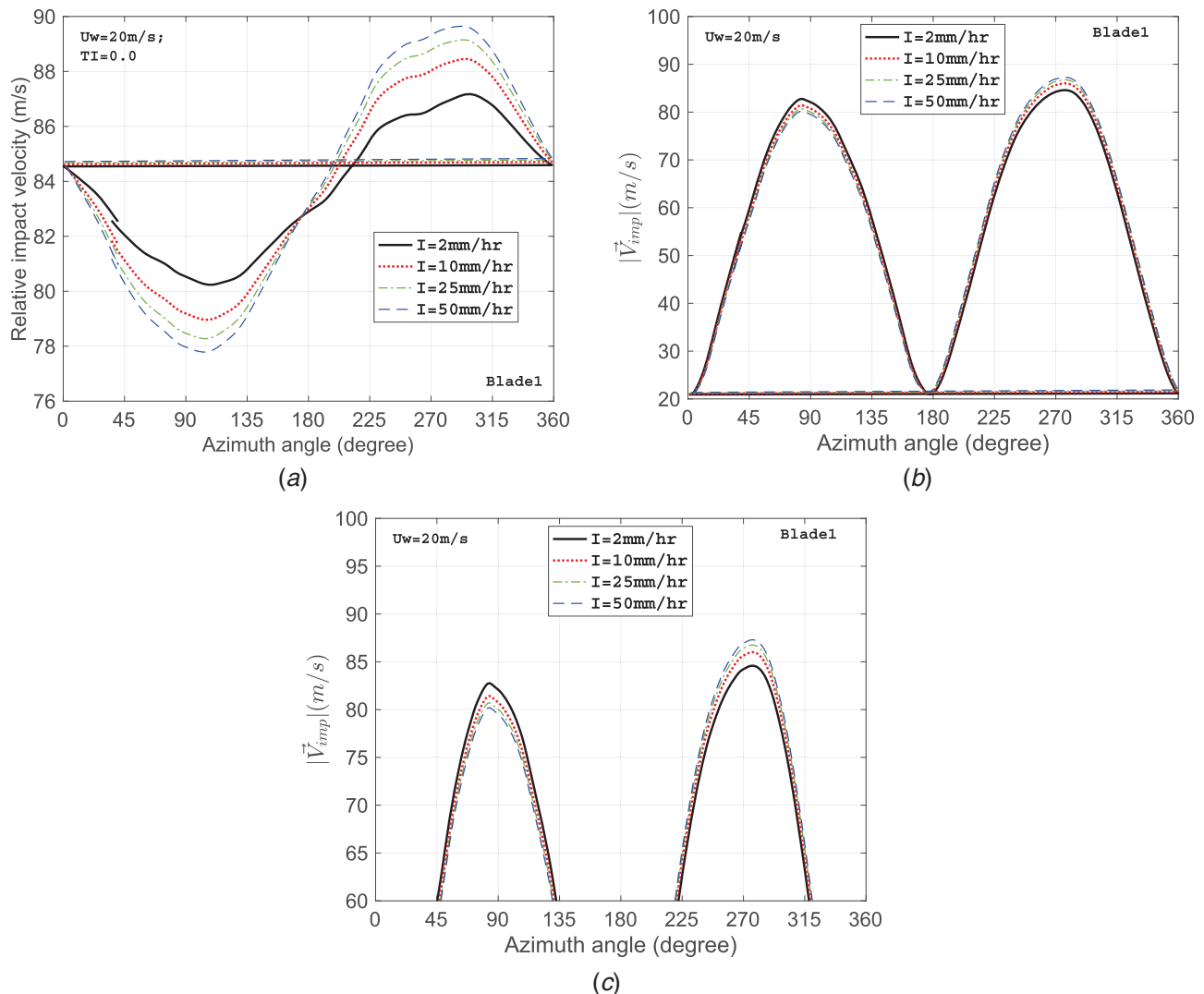


(a)



(b)



(c)

**Fig. 10** Comparison of (a) $|\vec{V}_{\text{imp}}|$ for $I = 2$ mm/h, 10 mm/h, 25 mm/h, 50 mm/h, (b) magnified view, and (c) comparison of $\dot{D}_i$

the impact velocity between the rotating blade tip ($r = 61.5$ m) and rain droplet corresponding to different values of $I = 2$ mm/h, 10 mm/h, and 25 mm/h, 50 mm/h, with the $V_x^{blade}$ component filtered out. The results are presented at different values of $\theta \in [0 \deg, 360 \deg]$ and for a case of an onshore WT operating at $U_w = 20$ m/s (i.e., above the rated wind speed) and having steady wind conditions ($TI = 0$). It can be seen from the figure that the impact velocity between the blade and the rain droplet varies cyclically, where it is least at approximately $\theta = 90$ deg and highest at approximately $\theta = 270$ deg. This trend is expected based on the results presented before in Figs. 9(a)–9(c), where $V_y^{blade}$ and $V_z^{blade}$ reached their negative peak values at $\theta = 270$ deg and thus contributed the most to the relative impact velocity. A magnified view is also presented in Fig. 10(c), showing the differences in the impact velocity for different rainfall intensities, which are found in the range of 2–5%. From the figure, there might be thoughts that there are not many differences in the impact velocities of the blade tip for different rainfall intensities and that only the blade tip speed dominates erosion while operating at a given wind speed. This is also represented in Fig. 11(a), where the rain droplet-induced water hammer pressure ($p_{wh}$) developed onto the blade at different blade azimuth angles (considering the material properties of the PET coating listed in Table 1) and for different $I = 2$ mm/h, 10 mm/h, 25 mm/h, and 50 mm/h is presented. The difference in $p_{wh}$ is minor and is found in the range of 2–5% for different $I$, given that $p_{wh}$ depends linearly on $\vec{V}_{imp}$.

However, it should be noted that the most important erosive parameter, i.e., the erosion damage rate ($\dot{D}_i$), is proportional to $\vec{V}_{imp}$ with a power of 6.7 (see Eq. (8)). In addition, the erosion damage rate ($\dot{D}_i$) is directly proportional to $q$, i.e., the number of droplets in a cubic volume of rain, and increases with increasing $I$. Therefore, even a modest increase in the impact velocity due to increasing rainfall intensity is expected to substantially increase the $\dot{D}_i$. This can be seen from Fig. 11(b), where the erosion damage rate is compared for the blade tip at different rainfall intensities, different $\theta$, and $U_w = 20$ m/s. The results clearly show that there is a substantial increase in the $\dot{D}_i$, which is more than 85% when exposed to very heavy rainfall compared to blades exposed to light rainfall. These results clearly demonstrate that for a given blade tip speed, different magnitudes of rainfall intensity are expected to have varying rain erosion performance. Thus, these aspects need to be considered when developing a control algorithm for reducing the tip speed of the blade. In this way, the incubation period ($1/\dot{D}_i$) of the blade can be extended. Figure 11(c) further presents the comparison between the peak impact forces caused between the rotating blade tip ($r = 61.5$ m) and rain droplet corresponding to different rainfall intensities ($I = 2$ mm/h, 10 mm/h, 25 mm/h, and 50 mm/h). Given that the peak force is proportional to $\vec{V}_{imp}$ and $\phi_d$ with a power of 2 (see Eq. (7)), a noticeable difference can be seen in the peak forces developed by heavy rainfall compared to light rainfall at different $\theta$. Overall, rainfall intensity is an essential parameter to be included in LEE analysis.
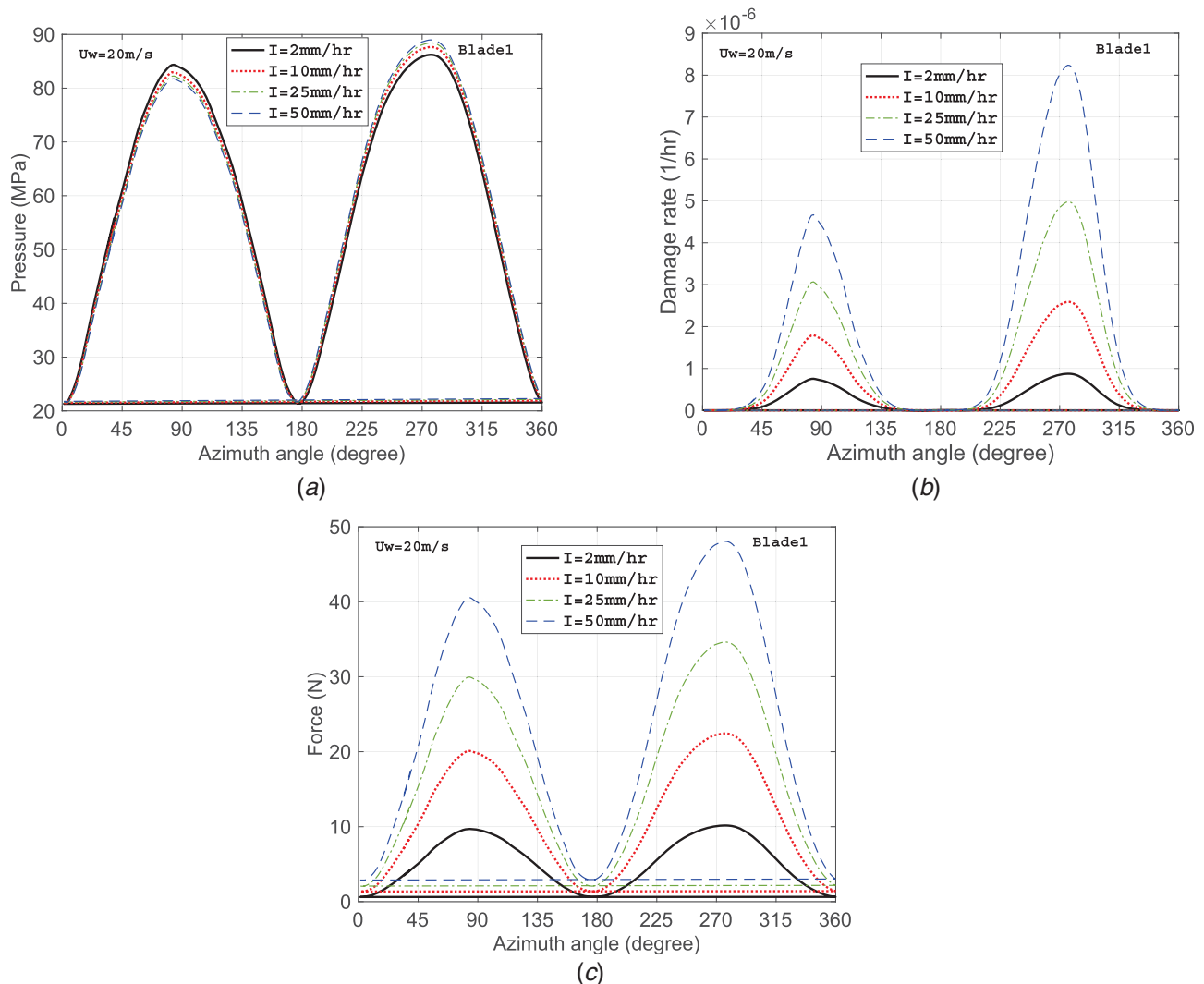


(a)



(b)



(c)

Fig. 11 Comparison of (a) $p_{wh}$, (b) $\dot{D}_i$, and (c) $F_{imp}$ for $I = 2$ mm/h, 10 mm/h, 25 mm/h, and 50 mm/h

**Effects of Wave-Induced Loads ($H_s$, $T_p$) on Tower Top Responses.** In this section, the effects of wave-induced loads on the LEE of WTBs in terms of $|\vec{V}_{imp}|$ and the erosion damage rate ($\dot{D}_i$) are discussed. Since collinear wind-wave conditions are considered in the study, only the motion of the monopile in the fore-aft direction will affect the results for $|\vec{V}_{imp}|$ and are discussed hereafter.

Figure 12(a) compares the motion of the tower top in the fore-aft direction (y-global) for a load case corresponding to $H_s = 2.30$ m, $T_p = 4.2$ s (EC2) and $H_s = 2$ m, $T_p = 12$ s (EC4) together with a constant $U_w = 6$ m/s, $TI = 0.06$ (below rated). It can be seen that the tower top has large responses in the fore-aft direction compared to $T_p = 12$ s and this is due to the fact that $T_p = 4.2$ s matches with the eigenfrequency of the turbine, thereby causing resonance. A spectral density curve for the tower top motion is compared for EC2 and EC4 in Fig. 12(b), where a high peak is seen at the resonance frequency for load case EC2. Nevertheless, the motion is still minor compared to the motion of the blade itself in the y-direction. This is due to the presence of aerodynamic damping from the rotating blades, which reduces the amplification of responses at resonance. For instance, Fig. 12(c) compares the motion of the tower top and blade in the global y-direction, and it is evident that the contribution of the monopile is minor. This implies that the wave-induced tower top motion is not expected to significantly change $V_y^{blade}$. This can be confirmed from Fig. 12(d), where $V_y^{blade}$ is compared for EC1, EC2, EC3, and EC4, where EC1

corresponds to the case of an onshore WT. The contribution of wave-induced loads is negligible, as the results for all the load cases completely overlap with each other except EC2, which exhibits a minor difference due to the resonance effects discussed above.

Subsequently, the impact forces and erosion damage rates are compared (Figs. 13(a) and 13(b)) between the onshore and offshore WTs for EC10. This case is the most critical for offshore WTs due to large wave heights ($H_s = 4.9$ m) and $T_p = 4.2$ s, which match the resonance frequency. These results are presented for two different rainfall intensities ($I = 2$ mm/h and 50 mm/h), the above rated wind speed ($U_w = 20$ m/s), and $TI = 0.12$. The results show that the differences in the impact forces and erosion damage rate are minor for onshore and offshore WTs under very heavy rainfall conditions and negligible for light, moderate, and heavy rainfall conditions. Overall, it can be implied from the results that LEE is not affected by wave-induced tower top responses; therefore, this parameter is not essential for LEE modeling. Note that the present paper only considers a monopile-based fixed offshore WT. These results will be compared in the future for floating offshore WTs.

**Effects of Turbulence Intensity.** In this section, the effects of turbulence intensity ($TI$) on the LEE are discussed. Figure 14(a) compares the velocity of the rotating blade in the global y-direction for three values of $TI = 0.0$, 0.12, 0.26 and $U_w = 20$ m/s. It is evident from the figure that considering only the steady wind for the LEE
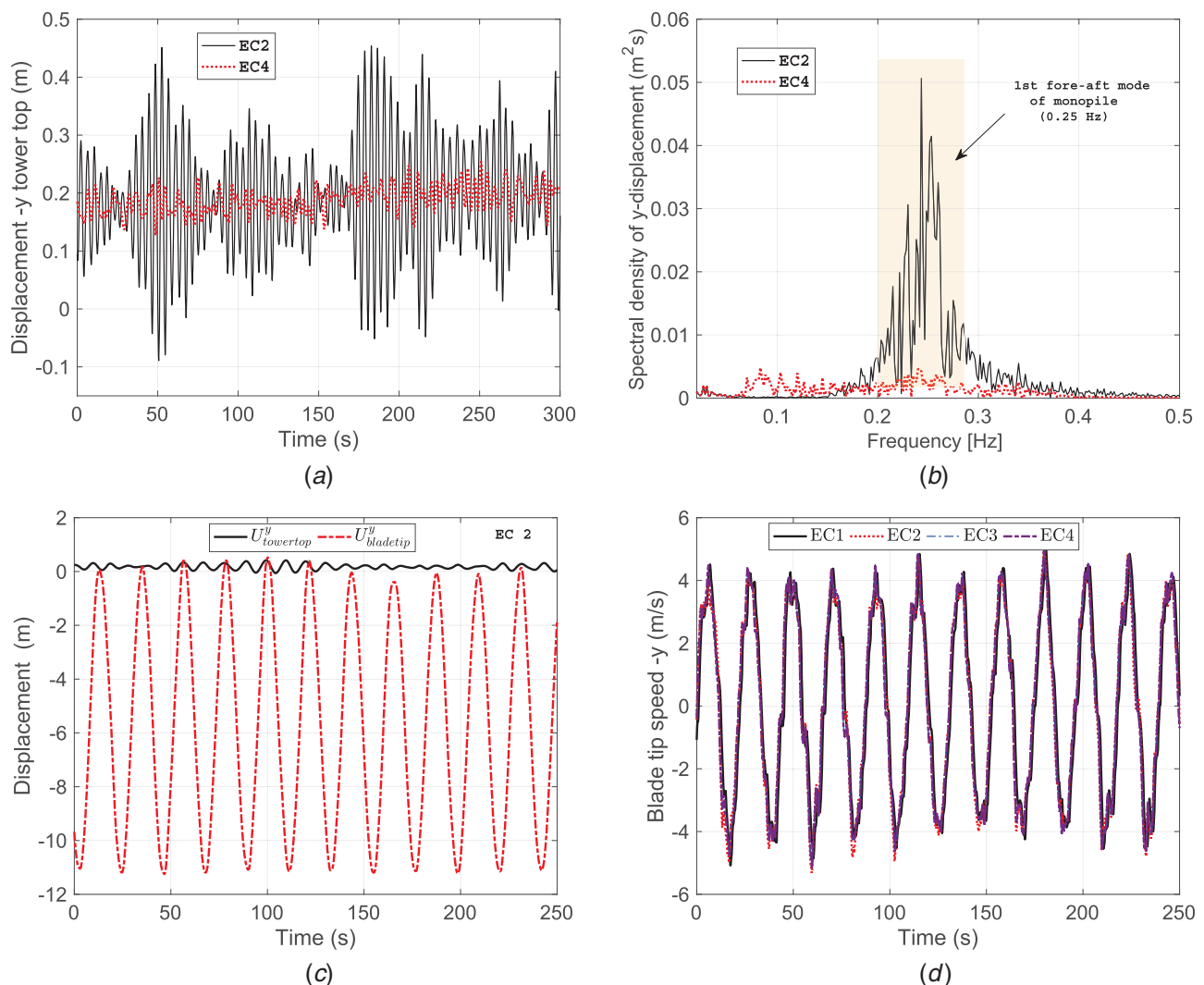


**Fig. 12 Comparison of (a) $U_{hub}^y$ and its (b) spectral density for EC2 and EC4; comparison of (c) $U_{hub}^y$ and $U_{blade}^y$; and (d) $V_y^{blade}$**
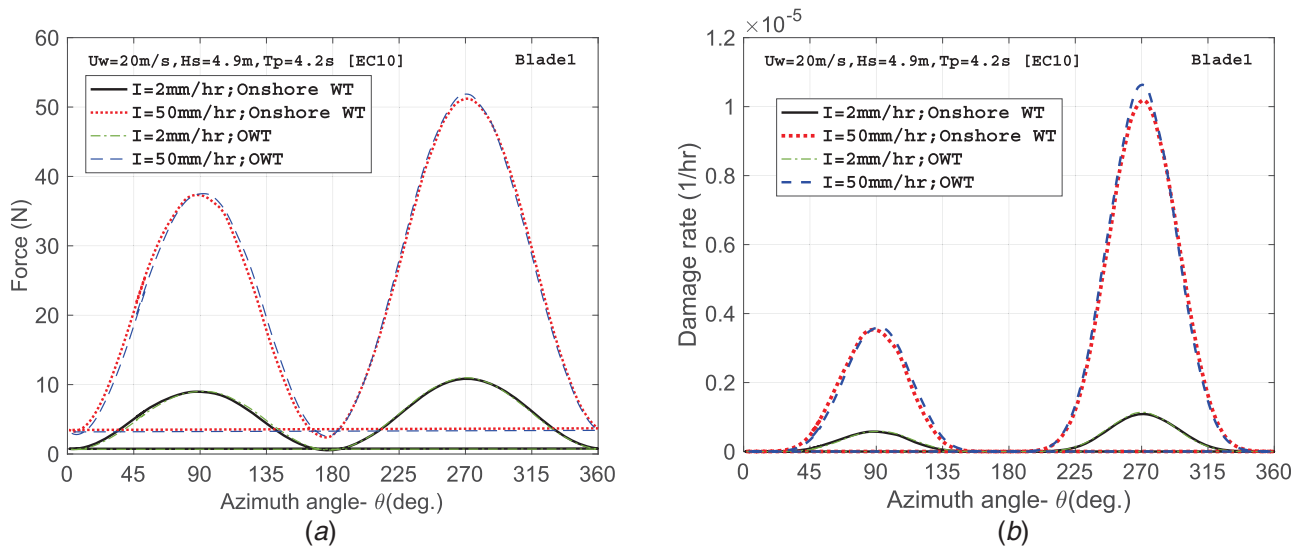
**Fig. 13 Comparison of (a) $F_{imp}$ and (b) $\dot{D}_i$ between onshore and offshore WT for EC10 ($H_s = 4.9$ m, $T_p = 4.2$ s, $U_w = 20$ m/s) and $I = 2$ mm/h, 50 mm/h**
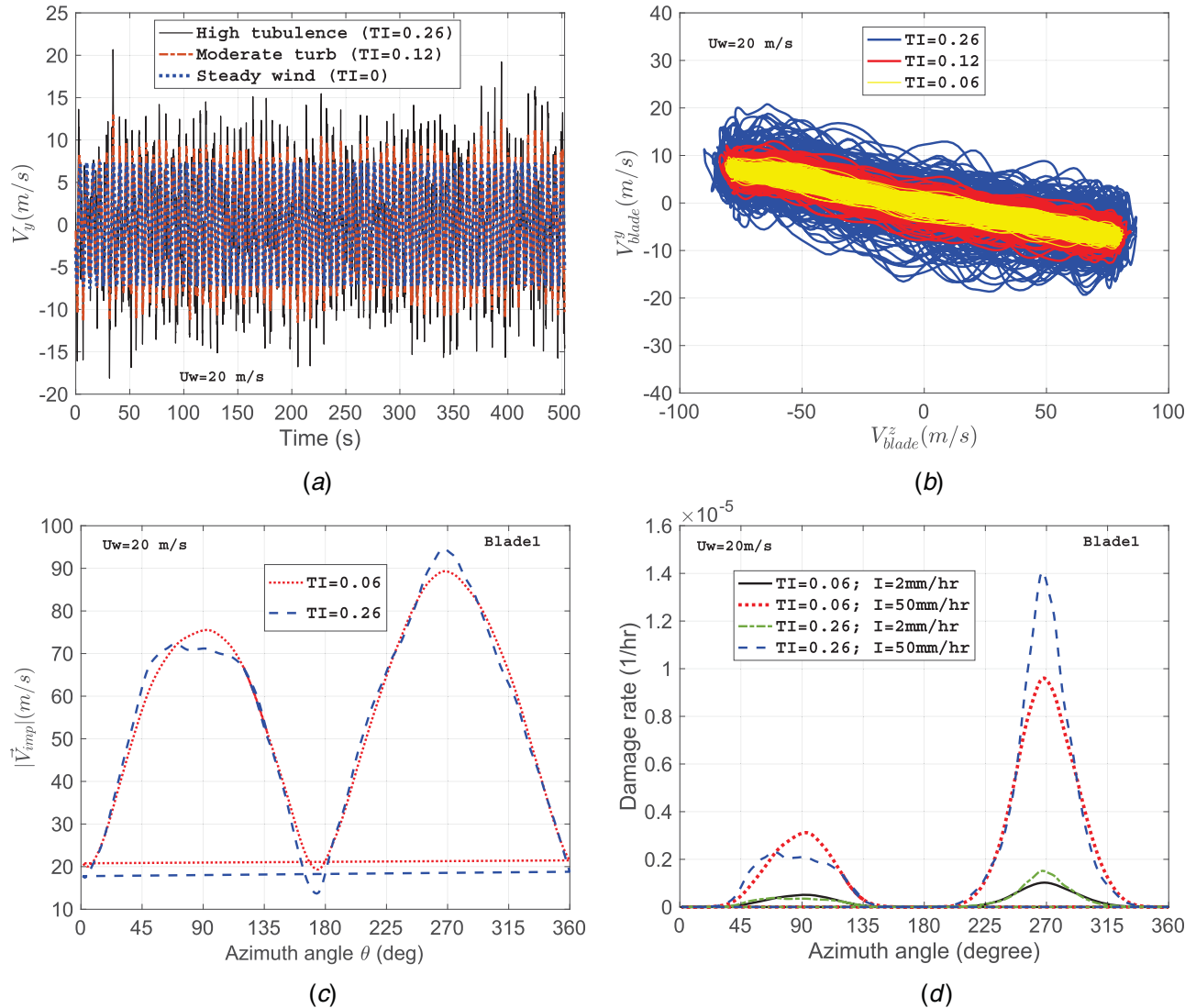


**Fig. 14 Comparison of (a) $V_y^{blade}$, (b) blade tip speed in $yz$-plane, (c) $|\vec{V}_{imp}|$, and (d) $\dot{D}_i$ for $TI = 0.06$, 0.26, $I = 2$ mm/h, 50 mm/h and $U_w = 20$ m/s**

analysis underpredicts $V_y^{\text{blade}}$. Furthermore, peak values for $V_y^{\text{blade}}$ increase from 7 m/s for $TI = 0.0$ to more than 20 m/s for $TI = 0.26$, thereby demonstrating the significance of $TI$ for LEE modeling. Similar observations can be seen in Fig. 14(b), where the velocity of the lifted blade in the critical $yz$-plane is compared for values of $TI = 0.06$, 0.12, 0.26 and $U_w = 20$ m/s. It can be seen from the figure that $V_y^{\text{blade}}$ increases with increasing $TI$, and there are minor influences on $V_z^{\text{blade}}$. Furthermore, Fig. 14(c) compares the $|\vec{V}_{\text{imp}}|$ for two $TI = 0.06$, 0.26 and at $\theta$. The difference in $|\vec{V}_{\text{imp}}|$ for both cases is minor; however, there is a substantial influence on the erosion damage rate of LE. Figure 14(d) compares the values of $\dot{D}_i$ for $TI = 0.06$, 0.26 and two rainfall intensities ($I = 2$ mm/h, 50 mm/h). The turbulence intensity is found to have a significant influence on the erosion damage rate, and the effect is most critical for very heavy rainfall conditions ($I = 50$ mm/h) and high turbulent wind associated with gust conditions ($TI = 0.26$). Overall, $TI$ is an important parameter to be included for LEE modeling. The results also show that the current state-of-the-art method, where the steady power curve of the WT is included for the LEE analysis, would underpredict the results.

**Effects of the Droplet Size Distributions Used for Representing Rainfall Scenarios at Onshore and Offshore Locations.** In our previous discussions, Best's DSD [23] was used to analyze LEE for representing rainfall scenarios at both onshore and offshore locations. This is because the distribution has been applied extensively in the literature for LEE. Nevertheless, a standalone comparative study is presented here to check the effect of the DSDs on the LEE of WTBs and to assess how site-specific rainfall conditions can affect the overall erosion damage rate. As discussed in "Material and Modeling Method" section, the rainfall scenario onshore is given by Best's DSD [23], whereas the rainfall scenario offshore is given by the DSD developed in Ref. [21]. In the onshore and offshore rain described through the above DSDs, the main distinction is the difference in the estimations of representative droplet sizes for a given rainfall condition. Thus, there will be distinct droplet sizes given the same rainfall intensity for onshore and offshore locations. For instance, an onshore rainfall representing light rainfall conditions ($I = 2$ mm/h) using Best's DSD represents rain comprising a median droplet size of 1.30 mm, whereas the same rainfall condition for offshore rain represents a relatively smaller median droplet size of 0.99 mm. Similarly, the very heavy rainfall condition ($I = 50$ mm/h) described by Best's DSD for onshore rain has a median droplet size of 2.34 mm, whereas for offshore rain $I = 50$ mm/h, and the droplet size is 1.48 mm.

Figure 15(a) compares the impact velocity between the rotating blade tip ($r = 61.5$ m) and a single rain droplet for onshore and offshore scenarios with two different values of $I$ ($I = 2$ mm/h and $I = 50$ mm/h). Each of these curves represents varying
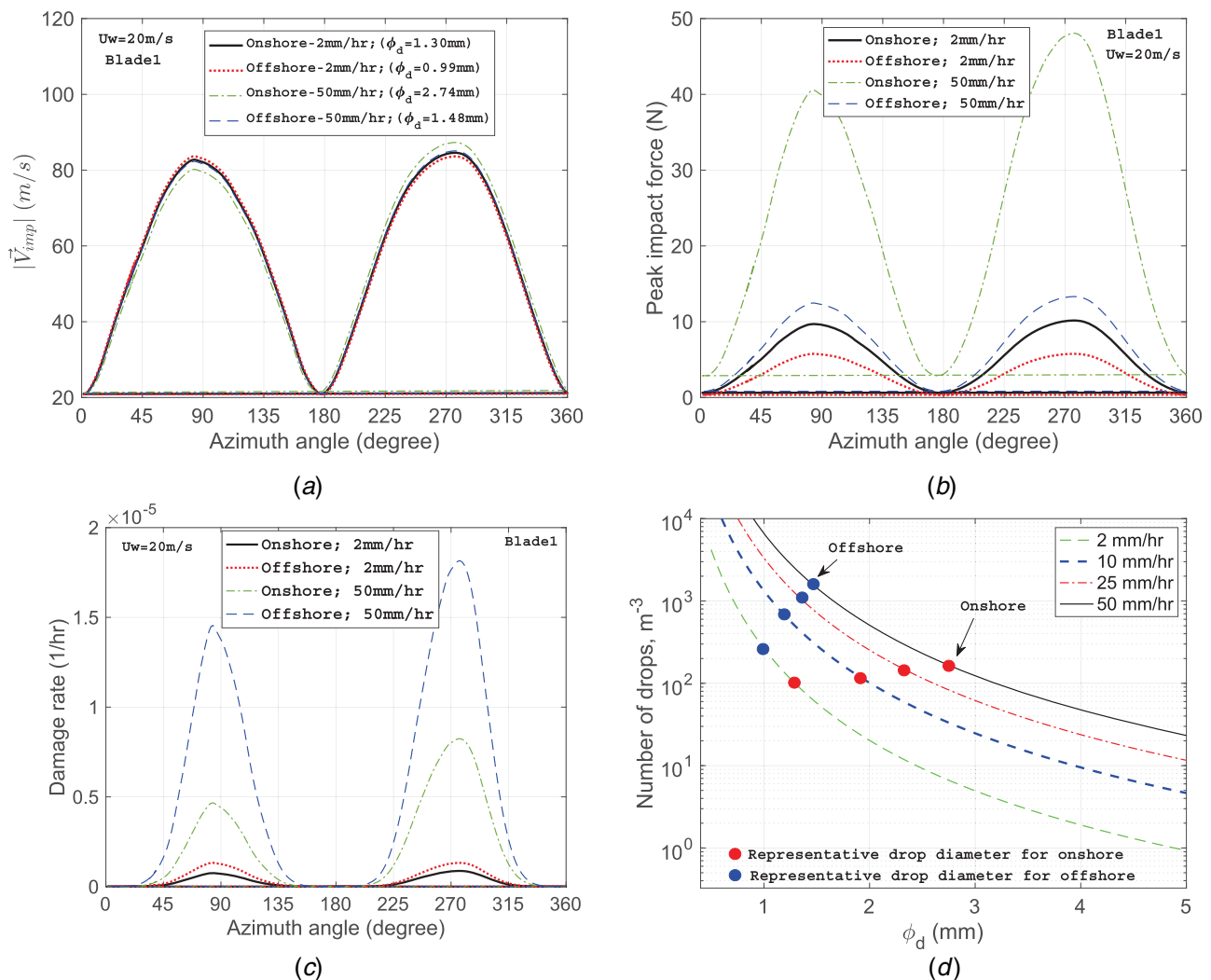


Fig. 15 Comparison of (a) $|\vec{V}_{\text{imp}}|$, (b) $F_{\text{imp}}$, (c) $\dot{D}_i$ for onshore and offshore rainfall condition $I = 2$ mm/h, 50 mm/h, and (d) q for several $\phi_d$ and $I = 2$ mm/h, 10 mm/h, 25 mm/h, 50 mm/h

median droplet sizes and different intensities of rain at onshore and offshore rainfall—median droplet sizes of 1.30 mm (light rainfall onshore), 0.99 mm (light rainfall offshore), 2.34 mm (very heavy rainfall onshore), and 1.48 mm (very heavy rainfall offshore). Furthermore, the results are presented for different $\theta \in [0 \text{ deg}, 360 \text{ deg}]$ and for a case of a WT operating at $U_w = 20$ m/s (i.e., above the rated wind speed) and having steady wind conditions ($TI = 0$). No wave-induced loads ($H_s$, $T_p$) are considered acting on the offshore WT to ensure a standalone comparison of the erosion damage rates due to varying DSDs. The figure shows that the values of the impact velocities for blade exposure to onshore and offshore rainfall scenarios differ slightly from each other for a given $I$. The impact velocities are found to be higher for the onshore scenario—the highest percentage difference between the $|\vec{V}_{\text{imp}}|$ for the onshore and offshore rainfall scenarios is in the range of 2–5% for very heavy rainfall conditions ($I = 50$ mm/h).This is because Best's distribution estimates a larger $\phi_d$ for a given rainfall intensity ($I$) and is associated with a higher terminal velocity of the droplet compared to the offshore DSD. These results are also reflected when comparing the peak impact forces (Fig. 15(b)) between the rotating blade tip ($r = 61.5$ m) and a single rain droplet (for onshore and offshore rainfall scenarios) for two different values of $I$ ($I = 2$ mm/h and $I = 50$ mm/h). Given that the peak impact force is proportional to $\vec{V}_{\text{imp}}$ and $\phi_d$ with a power of 2 (see Eq. (7)), a noticeable difference can be seen in the peak forces between the droplet and blade impact for onshore and offshore rainfall scenarios, with the largest value found for the case of an onshore DSD and for the highest $I$.

However, a very interesting result can be seen when comparing the erosion damage rates ($\dot{D}_i$) for a WTB exposed to onshore and offshore rainfall scenarios. Here, the erosion damage rate is calculated by considering the contribution from multiple rain droplets that are contained in a given rain scenario. The number of droplets in a given rain scenario is calculated according to Eq. (9), where it is assumed that the entire rainfall volume for a given intensity consists of rain droplets with diameters equal to the median droplet size. It can be seen from Fig. 15(c) that unlike the impact velocity and peak impact forces mentioned above, the erosion damage rate contributed from multiple rain droplets is found to be significantly large when exposed to the offshore rainfall scenario. The highest percentage difference between the $\dot{D}_i$ for onshore and offshore rainfall scenarios is found in the range of 100–110% for $I = 50$ mm/h. This is because $\dot{D}_i$ is directly proportional to $q$ (Eq. (8)), i.e., number of water droplets in a unit cubic volume of rain, which is significantly higher for the offshore rainfall scenario than that of onshore. Again, this is attributed to the fact discussed earlier that the offshore DSD predicts a much smaller droplet size ($\phi_d$) for a given $I$ compared to Best's DSD, thereby yielding more drops in a unit volume of rain. Note that $q$ in Eq. (9) is inversely proportional to the cubic power of $\phi_d$ and consists of $V_{tg}$ in the denominator with the $\phi_d$ term in an exponential function. Overall, even a modest change in the droplet size significantly influences $q$ and $\dot{D}_i$. For instance, Fig. 15(d) compares $q$ for different combinations of rainfall intensities and $\phi_d$. The number of drops in a given rain scenario using the offshore DSD for a given $I$ is notably larger than the onshore DSD (please note the $y$-axis, which is plotted on a logarithmic scale). This implies that during the blade rotation, low impact forces and pressures are developed due to single rain droplet impact for offshore conditions since offshore rain determined using the DSD from Ref. [21] consists of a smaller $\phi_d$ for a given $I$. However, there would be several such impacts (as $q$ is significantly larger) for a rainfall scenario described through offshore DSD compared to Best's DSD. This would cause a larger fatigue damage accumulation and erosion damage rate of a WTB due to exposure to rain. Overall, the rainfall scenario for offshore conditions, described based on the DSD in Ref. [21], is found to have a significant effect on the erosion damage rate of a WTB and is an essential parameter for modeling.

## Conclusions

The present paper performs aero-hydro-servo-elastic simulations on the rotating blade and investigates whether there are differences in erosion of blades due to (1) varying rainfall conditions modeled using different DSDs for onshore and offshore locations in combination with (2) winds of varying turbulence intensities and (3) wave-induced loads. The main aim of the study was to provide guidelines on whether all these environmental parameters must be included in LEE modeling. Different precipitation parameters for both onshore and offshore locations are considered through an in-house code, and erosion variables that include impact velocities, erosion damage rates, peak impact forces, and impact pressures are compared at different blade azimuth angles. An analytical surface fatigue damage model based on Springer's model [8] is considered together with fatigue properties for a PET-based thermoplastic leading edge coating. The following points are the main conclusions that are found through the analysis performed in the study regarding guidelines for environmental parameters to include for LEE modeling:

- The rainfall intensity ($I$) is an essential parameter for analyzing LEE of a WTB. The results from the study show that although there is a minor change in the impact velocity and impact pressure between individual rain droplets and rotating blades at different values of $I$ and blade azimuth angles, a substantial increase is found in the erosion damage rate ($\dot{D}_i$) of a WTB. The percentage difference in $\dot{D}_i$ of a WTB is more than 85% when exposed to very heavy rainfall compared to blades exposed to light rainfall. Overall, for a given blade tip speed and operating wind condition, different magnitudes of rainfall intensities are expected to have varying rain erosion performances.
- The turbulence intensity ($TI$) is also found to be an important parameter to include for LEE modeling and has rarely been considered in the literature. Again, the results show that the turbulence intensity minorly influences the impact velocity due to a single rain droplet impact; however, it has a substantial effect on the overall erosion damage rate due to multiple rain drops. For instance, for the investigated load cases, an 8% increase in the impact velocity is observed when the turbulence intensity increases from 6% to 26%, which demonstrates an increase in the erosion damage rate by more than 40%.
- An investigation is performed to check the effect of DSDs on the LEE of WTBs and to assess how site-specific rainfall conditions, described through different DSDs, can affect the overall erosion damage rate. The rainfall scenario onshore is given by Best's distribution [23], whereas the rainfall scenario offshore is given by the DSD developed in Ref. [21]. It was found that the erosion damage rate for a WTB is significantly larger when exposed to the offshore rainfall scenario compared to the onshore scenario—the highest percentage difference between the values of $\dot{D}_i$ for onshore and offshore rainfall scenarios is in the range of 100–110% for very heavy rainfall conditions ($I = 50$ mm/h). This is found because $\dot{D}_i$ is directly proportional to the number of water droplets in a unit cubic volume of rain and is significantly higher for the offshore rainfall scenario than that of onshore. Overall, DSDs are an important factor for LEE modeling.
- Finally, wave-induced loading is found to be an unimportant parameter to include for LEE modeling, and no substantial influence is found on LEE of a WTB. However, this conclusion is limited to a relatively stiff bottom fixed monopile-type offshore WT. In the future, similar investigations will be performed on floating offshore WTs.

## Limitations and Future Work

The investigations performed in this paper are limited to short-term analyses. Accurate evaluation of long-term LEE requires site-specific environmental data, information on the wind turbine

operational condition, and a probabilistic framework. These aspects will be considered in future work. Additionally, Springer's model [8] used in this study for estimating the erosion damage rate for the coating material needs to be validated and further improved by considering factors such as rest periods and viscoelastic properties of the elastomeric coatings. Furthermore, given that the atmospheric stability conditions vary for onshore and offshore conditions, their effects on the erosion damage rate will be investigated in further studies. Additionally, all these investigations and results will be compared in the future for floating-based offshore WTs.

## Acknowledgment

## Conflict of Interest

There are no conflicts of interest.

## References

[1] Verma, A. S., Vedvik, N. P., and Gao, Z., 2019, "A Comprehensive Numerical Investigation of the Impact Behaviour of n Offshore Wind Turbine Blade Due to Impact Loads During Installation," Ocean Engineering, 172, pp. 127–145.

[2] Verma, A. S., Jiang, Z., Vedvik, N. P., Gao, Z., and Ren, Z., 2019, "Impact Assessment of a Wind Turbine Blade Root During an Offshore Mating Process," Eng. Struct., 180, pp. 205–222.

[3] Verma, A. S., Jiang, Z., Ren, Z., Gao, Z., and Vedvik, N. P., 2019, "Response-Based Assessment of Operational Limits for Mating Blades on Monopile-Type Offshore Wind Turbines," Energies, 12(10), p. 1867.

[4] Verma, A. S., Vedvik, N. P., Haselbach, P. U., Gao, Z., and Jiang, Z., 2019, "Comparison of Numerical Modelling Techniques for Impact Investigation on a Wind Turbine Blade," Compos. Struct., 209, pp. 856–878.

[5] Verma, A. S., Zhao, Y., Gao, Z., and Vedvik, N. P., 2019, "Explicit Structural Response-Based Methodology for Assessment of Operational Limits for Single Blade Installation for Offshore Wind Turbines," Proceedings of the Fourth International Conference in Ocean Engineering (ICOE2018), Chennai, India, Feb. 18–21, Springer, pp. 737–750.

[6] Hofmann, M., and Sperstad, I. B., 2014, "Will 10 MW Wind Turbines Bring Down the Operation and Maintenance Cost of Offshore Wind Farms?" Energy Procedia, 53, pp. 231–238.

[7] Mishnaevsky, Jr., L., 2019, "Repair of Wind Turbine Blades: Review of Methods and Related Computational Mechanics Problems," Renewable Energy, 140, pp. 828–839.

[8] Springer, G. S., 1976, *Erosion by Liquid Impact*, John Wiley and Sons, New York, NY.

[9] Herring, R., Dyer, K., Martin, F., and Ward, C., 2019, "The Increasing Importance of Leading Edge Erosion and a Review of Existing Protection Solutions," Renew. Sustain. Energy Rev., 115, p. 109382.

[10] Wiser, R., Jenni, K., Seel, J., Baker, E., Hand, M., Lantz, E., and Smith, A., 2016, "Forecasting Wind Energy Costs and Cost Drivers: The Views of the World's Leading Experts," The Views of the World's Leading Experts; IEA: Paris, Germany.

[11] Slot, H., IJzerman, R., Nord-Varhaug, K., and van der Heide, E., 2018, "Rain Erosion Resistance of Injection Moulded and Compression Moulded Polybutylene Terephthalate PBT," Wear, 414, pp. 234–242.

[12] Keegan, M. H., Nash, D., and Stack, M., 2014, "Wind Turbine Blade Leading Edge Erosion: An Investigation of Rain Droplet and Hailstone Impact Induced Damage Mechanisms," Ph.D. thesis, University of Strathclyde, Glasgow.

[13] Eisenberg, D., Laustsen, S., and Stege, J., 2018, "Wind Turbine Blade Coating Leading Edge Rain Erosion Model: Development and Validation," Wind Energy, 21(10), pp. 942–951.

[14] Bech, J. I., Hasager, C. B., and Bak, C., 2018, "Extending the Life of Wind Turbine Blade Leading Edges by Reducing the Tip Speed During Extreme Precipitation Events," Wind Eng. Sci. Discuss., 3(2), pp. 729–748.

[15] Chen, J., Wang, J., and Ni, A., 2019, "A Review on Rain Erosion Protection of Wind Turbine Blades," J. Coat. Technol. Res., 16(1), pp. 15–24.

[16] Amirzadeh, B., Louhghalam, A., Raessi, M., and Tootkaboni, M., 2017, "A Computational Framework for the Analysis of Rain-Induced Erosion in Wind Turbine Blades, Part I: Stochastic Rain Texture Model and Drop Impact Simulations," J. Wind Eng. Ind. Aerodyn., 163, pp. 33–43.

[17] Verma, A. S., Castro, S. G., Jiang, Z., and Teuwen, J. J., 2020, "Numerical Investigation of Rain Droplet Impact on Offshore Wind Turbine Blades Under Different Rainfall Conditions: A Parametric Study," Compos. Struct., 241, p. 112096.

[18] Keegan, M. H., Nash, D., and Stack, M., 2013, "On Erosion Issues Associated With the Leading Edge of Wind Turbine Blades," J. Phys. D: Appl. Phys., 46(38), p. 383001.

[19] Castorrini, A., Corsini, A., Rispoli, F., Venturini, P., Takizawa, K., and Tezduyar, T. E., 2016, "Computational Analysis of Wind-Turbine Blade Rain Erosion," Comput. Fluids, 141, pp. 175–183.

[20] Verma, A. S., Castro, S. G., Jiang, Z., Hu, W., and Teuwen, J. J., 2020, "Leading Edge Erosion of Wind Turbine Blades: Effects of Blade Surface Curvature on Rain Droplet Impingement Kinematics," J. Phys.: Conf. Ser., 1618, p. 052003.

[21] Herring, R., Dyer, K., Howkins, P., and Ward, C., 2020, "Characterisation of the Offshore Precipitation Environment to Help Combat Leading Edge Erosion of Wind Turbine Blades," Wind Energy Sci. Discuss., 2020(5), pp. 1399–1409.

[22] De Lima, J., 1989, "The Influence of the Angle of Incidence of the Rainfall on the Overland Flow Process," Proc. 3rd IAHS Symp. New Directions for Surface Water Modeling, Baltimore. IAHS Publ. No. 181, Baltimore, MD, May.

[23] Best, A., 1950, "The Size Distribution of Raindrops," Q. J. R. Metereol. Soc., 76(327), pp. 16–36.

[24] Larsen, T. J., and Hansen, A. M., 2007, How 2 HAWC2, the user's Manual, Technical Report (Forskningscenter Risoe, Risoe).

[25] Jonkman, J., Butterfield, S., Musial, W., and Scott, G., 2009, "Definition of a 5-MW Reference Wind Turbine for Offshore System Development," National Renewable Energy Laboratory, Golden, CO, Technical Report No. NREL/TP-500-38060.

[26] Zhang, R., Zhang, B., Lv, Q., Li, J., and Guo, P., 2019, "Effects of Droplet Shape on Impact Force of Low-Speed Droplets Colliding With Solid Surface," Exp. Fluids, 60(4), p. 64.

[27] Zhang, B., Li, J., Guo, P., and Lv, Q., 2017, "Experimental Studies on the Effect of Reynolds and Weber Numbers on the Impact Forces of Low-Speed Droplets Colliding With a Solid Surface," Exp. Fluids, 58(9), p. 125.

[28] Jonkman, J., and Musial, W., 2010, "Offshore Code Comparison Collaboration (OC3) for Iea Wind Task 23 Offshore Wind Technology and Deployment," National Renewable Energy Laboratory (NREL), Golden, CO, Technical Report.

[29] Shirzadeh, R., Devriendt, C., Bidakhvidi, M. A., and Guillaume, P., 2013, "Experimental and Computational Damping Estimation of an Offshore Wind Turbine on a Monopile Foundation," J. Wind Eng. Ind. Aerodyn., 120, pp. 96–106.

[30] Morison, J., Johnson, J., and Schaaf, S., 1950, "The Force Exerted by Surface Waves on Piles," J. Petroleum Technol., 2(5), pp. 149–154.

[31] Hasselmann, K., 1973, "Measurements of Wind Wave Growth and Swell Decay During the Joint North Sea Wave Project (jonswap)," Deutschen Hydrografischen Zeitschrift, 8, pp. 95.

[32] Verma, A. S., Gao, Z., Jiang, Z., Ren, Z., and Vedvik, N. P., 2019, "Structural Safety Assessment of Marine Operations From a Long-Term Perspective: A Case Study of Offshore Wind Turbine Blade Installation," ASME 2019 38th International Conference on Ocean, Offshore and Arctic Engineering, Glasgow, Scotland, June 9–14.

[33] Madsen, H. A., Riziotis, V., Zahle, F., Hansen, M. O. L., Snel, H., Grasso, F., Larsen, T. J., Politis, E., and Rasmussen, F., 2012, "Blade Element Momentum Modeling of Inflow With Shear in Comparison With Advanced Model Results," Wind Energy, 15(1), pp. 63–81.

[34] Pirrung, G. R., Madsen, H. A., Kim, T., and Heinz, J., 2016, "A Coupled Near and Far Wake Model for Wind Turbine Aerodynamics," Wind Energy, 19(11), pp. 2053–2069.

[35] Mann, J., 1994, "The Spatial Structure of Neutral Atmospheric Surface-Layer Turbulence," J. Fluid Mech., 273, pp. 141–168.

[36] Ren, Z., Skjetne, R., Verma, A. S., Jiang, Z., Gao, Z., and Halse, K. H., 2021, "Active Heave Compensation of Floating Wind Turbine Installation Using a Catamaran Construction Vessel," Marine Struct., 75, p. 102868.